Scientia Iranica B (2022) 29(5), 2271–2278

Sharif University of Technology
Scientia Iranica
Transactions B: Mechanical Engineering
http://scientiairanica.sharif.edu

Research on semi-random track irregularity of straddle type monorail

Zh. Xu*, Z. Du, Zh. Yang, and L. Xin

School of Mechanotronics and Vehicle Engineering, Chongqing Jiaotong University, No. 66, Xuefu Road, Nan' an District, Chongqing, 400074, China.

Received 28 July 2019; received in revised form 18 January 2022; accepted 25 April 2022

KEYWORDS
Straddle type monorail;
Running surface;
Track irregularity;
Semi-random;
Real vehicle test.

Abstract. The dynamic performance of a straddle monorail train highly depends on the track irregularity. However, limited research on the track irregularity and semi-random particularity of straddle monorails has made the application of the existing track spectrum impossible. In this respect, the current study aims to measure the irregularity of the running surface of Prestressed Concrete (PC) beam of monorail, draw the altitude map, and determine the expression of the track random irregularity. To this end, the irregularity of the finger-band and deflection of PC beam under a dead load were studied, and a method was proposed to describe the semi-random track irregularity of the straddle type monorail. Finally, the running surface of the straddle monorail was reconstructed, and its accuracy was verified through a comparison of the obtained and test results.

1. Introduction

As a typical urban rail transit system, straddle monorail is widely used in China. As the most important excitation, the accuracy of track irregularity seriously affects the analysis results such as stability, structural strength, safety, and comfortability [1].

The structure of the straddle monorail vehicles is quite complex; each car has four running wheels, eight guide wheels, and four stability wheels, all of which are rubber tires. The tracks are composed of Precast Concrete (PC) beams that are connected by finger bands [2]. Due to the vehicle structure and track characteristics, description of the irregularity of the straddle monorail cannot copy the rail or ordinary road. Of note, the author has not yet found relevant literature on the irregularity assessment of the track of straddle monorail.

On the contrary, numerous researches addressed road or rail irregularity. In recent years, several researchers have studied the application of new sensors and reconstruction of irregularity; however, they have not mentioned how to describe the track irregularity with strong regularity, such as straddle monorail track. Among these researchers, Ngwangwa et al. [3], Zhang et al. [4], and Cantisani and Loprencipe [5] examined the problem of how to obtain road roughness and mutual excitation between the vehicle and road surface. In addition, Yuan et al. [6], Kumar et al. [7], and Han, et al. [8] investigated the method for the application of laser sensors to measure road roughness. Cheli and Corradi [9], Mucka [10], and Zhu et al. [11] studied the coherent function model of track irregularity as well as the interaction between the track and train. Jiang et al. [12], Lee et al. [13], Chen et al. [14],

*. *Corresponding author. Tel.: +8613368064998*
E-mail addresses: xuzhouzhou@hotmail.com (Zh. Xu); aaadzx@163.com (Z. Du); 21930315@qq.com (Zh. Yang); xinlaero@163.com (L. Xin)

doi: 10.24200/sci.2022.53909.3602

and Leng et al. [15,16] assessed the related algorithm and reconstruction of the monorail track irregularity.

Track irregularity has been widely investigated by studies done on the straddle monorails including road or rail irregularity. Nevertheless, their practicality or appropriateness has not been examined yet. Zhou et al. [17,18], Wen et al. [19], and Du et al. [20–22] evaluated the traction performance, curve passing performance, stability, structural strength, and safety and comfort of the straddle monorail trains under the excitation of A-level road roughness. Further, Lee et al. [23], Yulong et al. [24,25], and Cai et al. [26] discussed the dynamic response analysis procedure considering the traffic-induced vibration of a monorail bridge and train.

In order to compensate the lack of an expression method regarding the irregularity of regular tracks, a solution was proposed and its feasibility was verified through the experiments.

2. Measurement of track irregularity

In order to acquire the first-hand data and provide support for the follow-up research, the paper tested the inequality of the PC beams for straddle monorails.

2.1. Measuring principle

In the mentioned test, non-contact method and laser rangefinder were used to measure the altitude of the running surface of the PC beams. As depicted in Figure 1, the scanner was first fixed on a bracket of about 1.2 m high from the surface of the PC beam and then, the distance L and angle θ from the laser rangefinder to the points on the surface were measured to obtain the coordinates of each point on the road surface of the PC beam based on Eq. (1). The descriptions of the following symbols are given in nomenclature.

$$x_{i,j} = l_{i,j} * \sin\theta,$$

$$y_{i,j} = l_{i,j} * \cos\theta,$$

$$A_i = \{(x_{i,1}, z_{i,1}), (x_{i,2}, z_{i,2}) \cdots (x_{i,147}, z_{i,147})\}. \tag{1}$$

2.2. The irregularity test of the running surface of the PC beams

In this study, the PC beams used in Chongqing Rail Transit Line 3 were investigated in the PC beam depository in Yudong. In doing so, 15 PC beams were selected, each of which was about 22 meters long. The beams were supported at both ends and placed on the ground. According to ISO8608, the distance between the adjacent data points is 0.15 m (x direction); then, 147 datasets can be measured for each PC beam. The laser ranging sensor adopts LMS151 of SICK with the measurement range of 0.5–50 m, angular resolution of 0.25°, and statistical error of 12 mm (Figure 2).

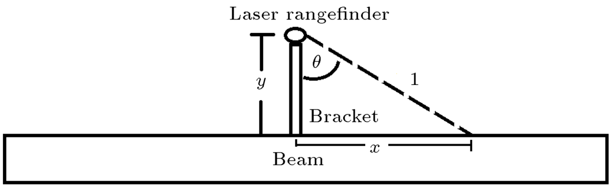

Figure 1. Measuring principle.

Figure 3 presents the data of several PC beams. As observed, their surfaces are relatively smooth but their cambers are obvious, and the middle part, compared with the two ends, protrudes about 32 mm.

3. Calculation of track irregularity of straddle type monorail based on road spectrum

The author constructs a road using seven PC beams (Figure 4), which is 154 meters long and includes 1024 data points, similar to Eq. (2), where the value of i ranges from 1 to 7.

$$x'_{i,n} = 0.15[147(i-1) + (n-1)],$$

$$z'_{i,n} = z_{i,n} + (z'_{i-1,147} - z_{i,1}). \tag{2}$$

According to ISO8608, Power Spectral Density (PSD) of the road based on the spatial frequency $\{G_d(n_k), n_k\}$ can be calculated based on Eq. (3):

$$n_c = 2^n,$$

$$\begin{cases} n = k, & -7 \le n \le -5, \quad -7 \le k \le -5 \\ n = \frac{k}{3}, & -5 \le n \le -2, \quad -15 \le k \le -6 \\ n = \frac{k}{12}, & -2 \le n \le 1.75, \quad 24 \le k \le 21 \end{cases}$$

$$G_d(n_c) = \text{average}(G_d(j)),$$

$$\frac{n_{c-1} + n_c}{2} \le j \le \frac{n_{c+1} + n_c}{2}. \tag{3}$$

Followed by curve fitting, the displacement PSD function of the road can be obtained based on Eq. (4) and Figure 5. It belongs to the A-class road.

$$G_d(n) = 1.08 \times 10^{-8} \times \left(\frac{n}{0.2806}\right)^{-0.719}. \tag{4}$$

4. Study on the road profiles of straddle type monorail

As observed in Figure 5, there is a big pulse at a position of 0.045 m^{-1}, which is originated from the beam camber. While considering the effect of the finger band, the pulse is larger. However, when considering the displacement PSD function of the road, this pulse will be eliminated.

(a) The laser ranging sensor

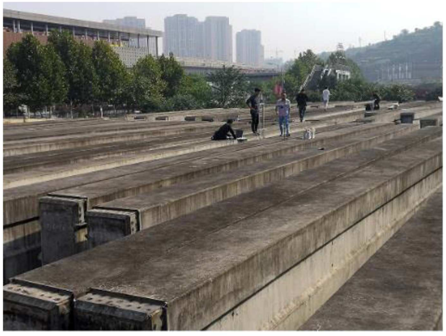

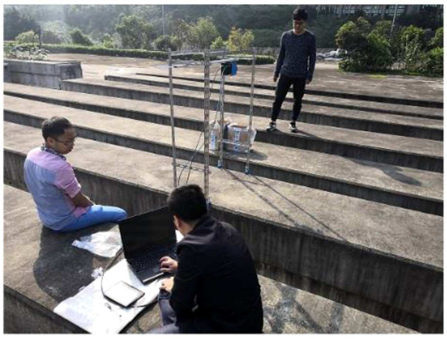

(b) The beam yard (c) The test

Figure 2. Track surface irregularity measurement.

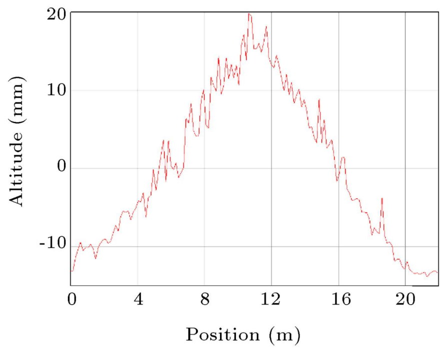

(a) The first beam

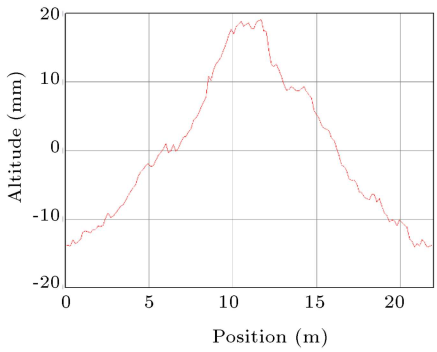

(b) The fourth beam

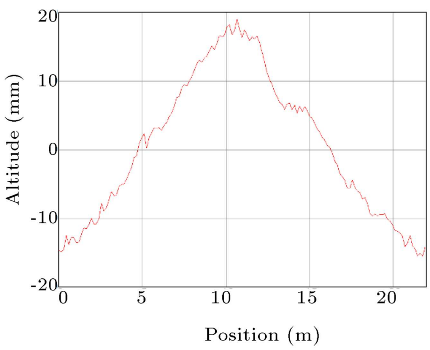

(c) The eighth beam

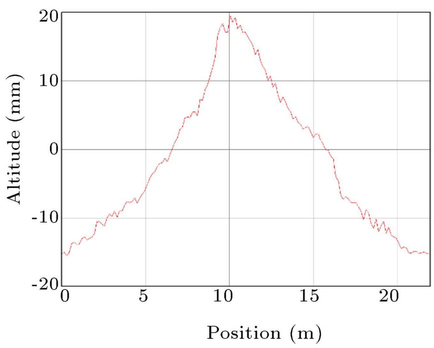

(d) The twelfth beam

Figure 3. The altitudes of some of the track beams.

Given the particularity of straddle monorail roads, the track profiles must contain the following elements: the irregularity (excluding the beam camber), beam camber, and span of PC the beam as well as the clearance of the finger-band (in Figure 6), as suggested in Eq. (5):

$$z(x) = q(x) + y(x) + f(x). \tag{5}$$

The value of $q(x)$ can be obtained from ISO8608, which is not described here. Here, $y(x)$ can be defined through Eq. (6) where $w = 32$, and $f(x)$ is defined by Eq. (7) [27]:

$$y(x)=\begin{cases} w-\frac{2w}{l}\left|x-nl-\frac{1}{2}l\right| & \text{when } cl\leq x\leq (n=1)l \\ 0 & \text{when } x \text{ takes other values} \end{cases} \tag{6}$$

$$f(x)=\begin{cases} -10 & \text{when } nl-u-\frac{d}{2}\leq x\leq nl-\frac{d}{2} \\ -10 & \text{when } nl+\frac{d}{2}\leq x\leq nl+\frac{d}{2}+u \\ 0 & \text{when } x \text{ takes other values} \end{cases} \tag{7}$$

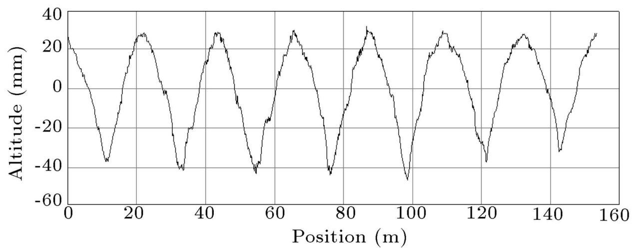

Figure 4. Combined road.

Based on the instructions given in Eq. (5), the 155-meter-long track was built using the value of $q(x)$ obtained from considering the A-class pavement roughness, as shown in Figure 7.

5. Test verification

From 1:00 to 5:00 a.m. on October 27, 2017, a train test was conducted at Tongyuan Bureau to Longtousi Section of Chongqing Railway Line 3. The vehicle was loaded with counterweight to simulate AW3 working conditions, and the vibration acceleration of different points of the middle car was measured (Figure 8). The sampling frequency of the accelerometer used in the experiment was 2000 Hz, and a relatively straight section of the line was selected for comparison. The travel distance and time were about 1000 m and 100 s, respectively.

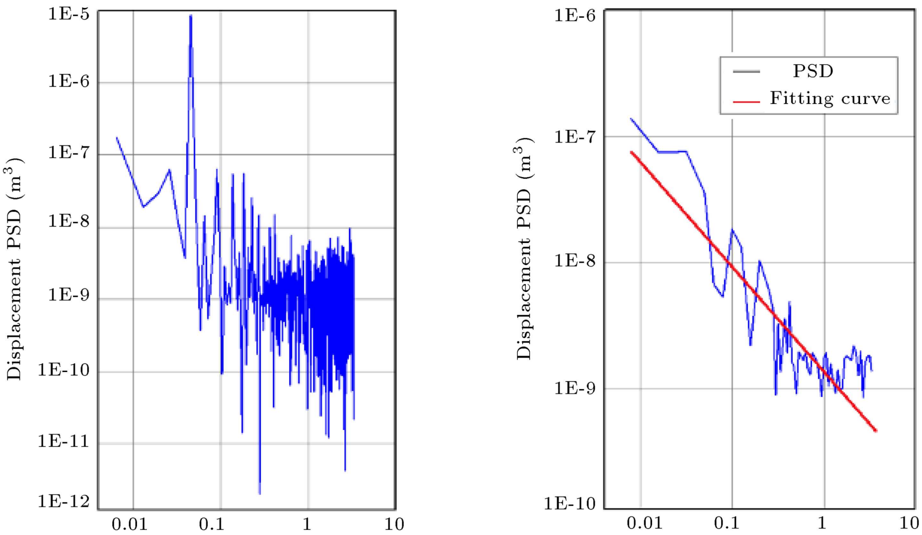

(a) The PSD before smoothing (b) The PSD after smoothing

Figure 5. Roughness of the roads.

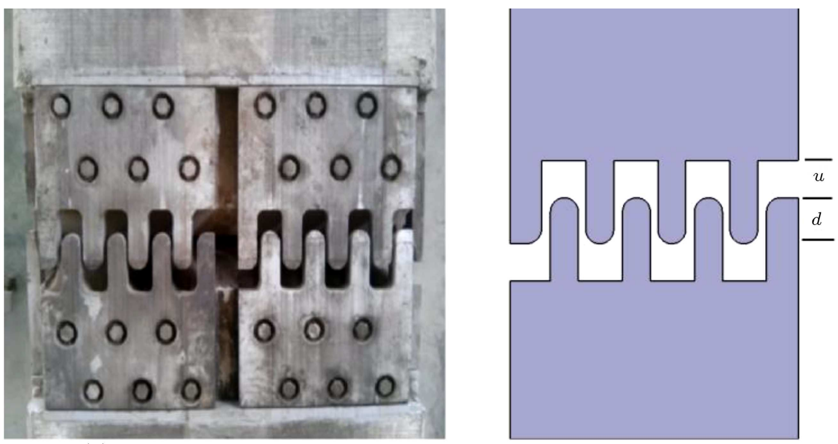

(a) The photo of finger-band (b) Structural model of finger-band

Figure 6. The finger-band.

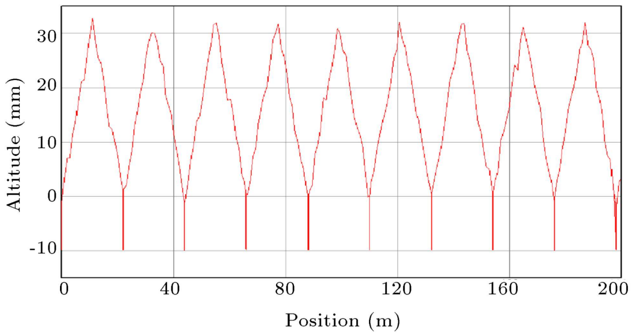

Figure 7. The irregularity of the track.

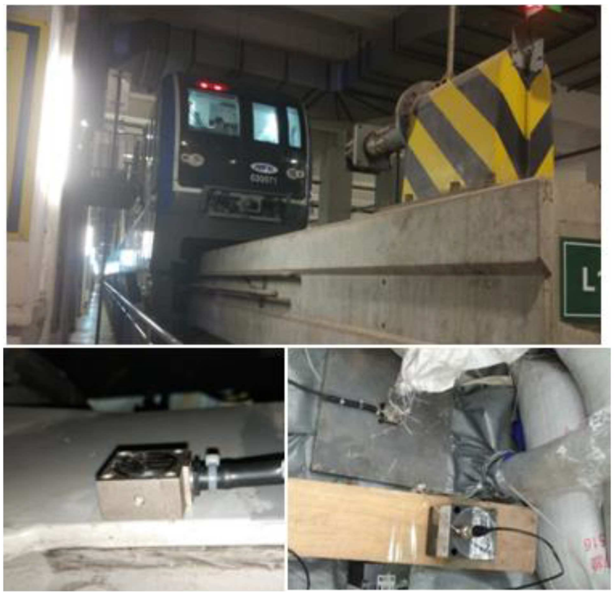

Figure 8. The test of the train.

In the simulation, the car body adopted the vehicle model of Chongqing Line 3 (Figure 9), and the relative parameters are listed in Table 1. For comparison, two simulations were carried out among which the first simulation used road spectrum only and the second one used the irregularity obtained from Figure 7.

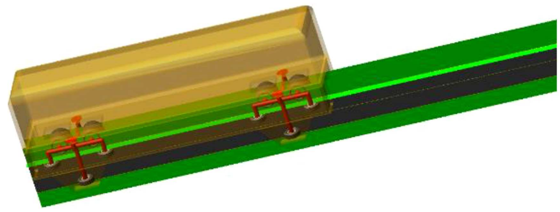

Figure 9. Vehicle simulation model.

Given that bogie is the most representative part of wheel rail contact, this study compared the vertical acceleration and FFT values at the center of the front bogie of the vehicle. The simulation results, considering the ordinary road profiles only, were quite different from those of the actual situation; however, the results were similar to those of the actual situation when using the track irregularity given in Eq. (5), especially when several characteristic vibration frequencies were almost the same.

According to Figure 10, in the case of using only A-level pavement spectrum for simulation, the vertical vibration of the train will be significantly less than that of the test. However, followed by incorporating of the finger-band and camber of the track beam, the vertical vibration amplitude of the train calculated by simulation will be almost the same as that of the test.

Figure 11 depicts the frequency domain diagram of the vertical vibration of the bogie according to which while considering the A-level road roughness (Figure 11(a)), the vibration amplitude of the train bogie becomes quite small and the wave peaks at 2.01 Hz and 2.22 Hz correspond to the natural frequency of the bogie. This finding is very different from that of the test. Followed by adding the finger plate excitation and track beam camber, the first-order frequency calculated by simulation is 3.51 Hz, which is very close to 3.60 Hz obtained from the test. Track irregularity is proved

Table 1. Car dynamics parameters.

Project	Value	Project	Value
Body mass in AW3 (kg)	25800	Running wheel mass (kg)	54
Bogie mass (kg)	5600	Guide wheel mass (kg)	30
Rotational inertia of body I_{xx} (kg.m^2)	43000	Vertical stiffness of the running wheel (N/m)	1200000
Rotational inertia of body I_{yy} (kg.m^2)	365000	Vertical damping of the traveling Wheel (N.s/m)	3400
Rotational inertia of body I_{zz} (kg.m^2)	365000	Radial stiffness of the guide wheel (N/m)	980000
Rotational inertia of bogie I_{xx} (kg.m^2)	2400	Radial damping of the guide Wheel (N.s/m)	3120
Rotational inertia of bogie I_{yy} (kg.m^2)	3400	Vertical stiffness of air spring (N/m)	160000
Rotational inertia of bogie I_{zz} (kg.m^2)	9600	Longitudinal stiffness of the traction rubber stack (N/m)	490000

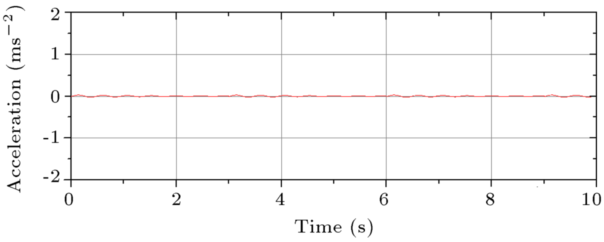

(a) The first simulating data

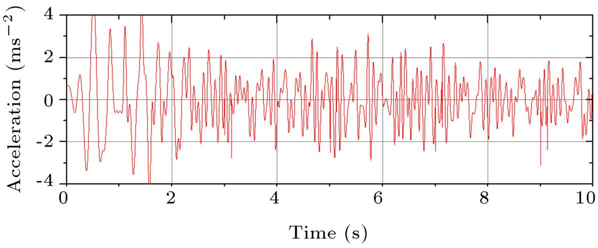

(b) The second simulating data

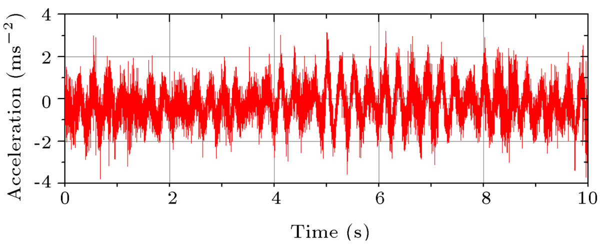

(c) The experimental data

Figure 10. Vertical vibration acceleration at the center of the front bogie.

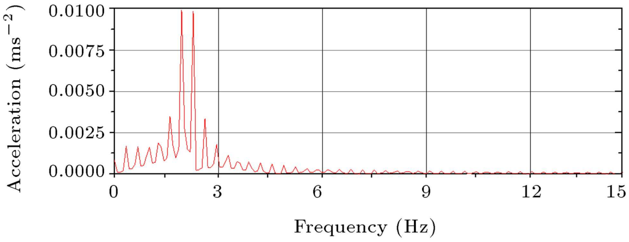

(a) The first simulation data

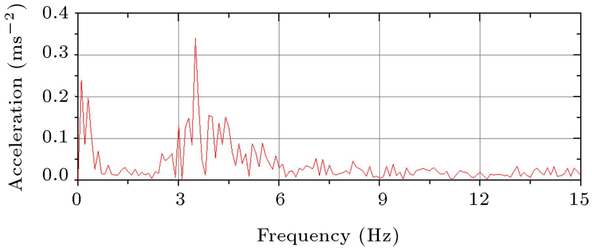

(b) The second simulation data

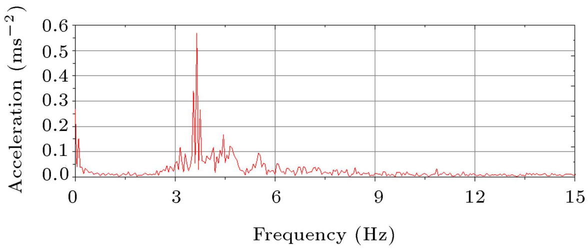

(c) The experimental data

Figure 11. FFT of the vertical vibration acceleration at the center of the front bogie.

to be the main cause of the vertical vibration of the straddle monorail train, thus verifying the accuracy of Eq. (6).

6. Conclusion

The current research used a statistical value to clearly describe the track and road irregularity that can better reflect the surface random irregularity. However, it ignored the regular irregularity of the surface as the main cause of a large error in the surface dynamic calculation with strong regularity. Followed by taking the straddle monorail as an example in this study, a method for expressing track irregularity with strong regularity was proposed, and its feasibility was verified through experiments. The findings of this study are summarized as follows:

1. It is suggested that track irregularity be composed of random irregularity and regular irregularity, hence establishment of the expression method of track irregularity of straddle monorail;
2. This study succeeded in completing the irregularity test of the running surface of PC beams used for straddle monorail for the first time and calculating the random irregularity of the track. In addition, it evaluated the periodic impacts of the track such as the beam camber and finger-band and established the expression of periodic track irregularity;
3. The irregularity of the track of Chongqing Rail Transit Line 3 was reconstructed in this study, and the required dynamic simulation calculation was carried out. The comparison between the findings and test results verified the accuracy of the description method for the pavement unevenness of straddle type monorail.

Nomenclature

$x_{i,j}$	The abscissa of the jth point of the ith beam
A_i	The coordinate set of all the points of the ith beam
$G_d(\cdot)$	Displacement PSD
$z(x)$	The altitude of the track at X coordinate
$y(x)$	The influence of camber of the beam
w	The maximum settlement of measured deflection under dead load
l	The span of PC beam

$y_{i,j}$	The ordinate of the jth point of the ith beam
$z_{i,n}$	The altitude of the jth point of the nth beam
n_c	The cth spatial frequency
$q(x)$	Random irregularity of track
$f(x)$	The influence of finger-bands
e	The width of fingertip gap; d is the length of interlaced fingers
d	The length of interlaced fingers

References

1. Naeimi, M., Tatari, M., Esmaeilzadeh, A., et al. "Dynamic interaction of the monorail-bridge system using a combined finite element multibody-based model", *Proceedings of the Institution of Mechanical Engineers Part K Journal of Multi-body Dynamics*, **229**(K2), pp. 132–151 (2014).

2. Zhong, J.H., *Structure and Analysis of Turnout for Straddle Type Monorail Traffic Vehicle*, China Communications Press (2013).

3. Ngwangwa, H.M., Heyns, P.S., Labuschagne, F.J.J., et al. "Reconstruction of road defects and road roughness classification using vehicle responses with artificial neural networks simulation", *Journal of Terramechanics*, **47**(2), pp. 97–111 (2010).

4. Zhang, Z.M., Deng, F.D., Huang, Y., et al. "Road roughness evaluation using inpavement strain sensors", *Smart Materials & Structures*, **24**(11), 115029 (2015).

5. Cantisani, G. and Loprencipe, G. "Road roughness and whole body vibration: evaluation tools and comfort limits", *Journal of Transportation Engineering*, **136**(9), pp. 818–826 (2010).

6. Yuan, Z., Zhang, X., Liu, S., et al. "Laser line recognition for autonomous road roughness measurement", *2015 IEEE International Conference on CYBER Technology in Automation IEEE* (2015).

7. Kumar, P., Lewis, P., Mcelhinney, C., et al. "An algorithm for automated estimation of road roughness from mobile laser scanning data", *The Photogrammetric Record*, **30**(149), pp. 30–45 (2015).

8. Han, W., Yuan, S., and Ma, L. "Vibration of vehicle-bridge coupling system with measured correlated road surface roughness", *Structural Engineering & Mechanics*, **51**(2), pp. 315–331 (2014).

9. Cheli, F. and Corradi, R. "On rail vehicle vibrations induced by track unevenness: Analysis of the excitation mechanism", *Journal of Sound & Vibration*, **330**(15), pp. 3744–3765 (2011).

10. Mucka, P. "Model of coherence function of road unevenness in parallel tracks for vehicle simulation", *International Journal of Vehicle Design*, **67**(1), p. 77 (2015).

11. Zhu, Z., Wang, L., Costa, P.A., et al. "An efficient approach for prediction of subway train-induced ground vibrations considering random track unevenness", *Journal of Sound and Vibration*, **455**, pp. 359–379 (2019).

12. Jiang, Y., Wu, P., Zeng, J., et al. "Simplified and relatively precise back-calculation method for the pavement excitation of the monorail", *International Journal of Pavement Engineering*, **22**(4), pp. 480–497 (2019).

13. Lee, C.H., Kim, C.W., Kawatani, M., et al. "Dynamic response analysis of monorail bridges under moving trains and riding comfort of trains", *Engineering Structures*, **27**(14), pp. 1999–2013 (2005).

14. Chen, Z., Xu, L., and Zhai, W. "Investigation on the detrimental wavelength of track irregularity for the suspended monorail vehicle system", *Railway Development, Operations, and Maintenance*, pp. 161–168 (2018).

15. Leng, H., Ren, L., Ji, Y., et al. "A newly designed coupled-bogie for the straddle-type monorail vehicle: calculation method for the key parameter and dynamic performance", *Advances in Dynamics of Vehicles on Roads and Tracks, IAVSD 2019*, pp. 541–550 (2020).

16. Leng, H., Ren, L., Ji, Y., et al. "Radial adjustment mechanism of a newly designed coupled-bogie for the straddle-type monorail vehicle", *Vehicle System Dynamics*, **58**(9), pp. 1407–1427 (2019).

17. Zhou, J., Du, Z., Yang, Z., et al. "Dynamic parameters optimization of straddle-type monorail vehicles based multiobjective collaborative optimization algorithm", *Vehicle System Dynamics*, **58**(3), pp. 357–76 (2020).

18. Zhou, J., Du, Z.X., Yang, Z., et al. "Dynamic parameters optimization of straddle-type monorail vehicles based multiobjective collaborative optimization algorithm", *Vehicle System Dynamics*, **58**(3), pp. 357–376 (2019).

19. Wen, X., He, Y.T., and Du, Z.X. "Crash simulation of straddle-type monorail vehicle body and human injury research", *Advanced Materials Research*, **413**, pp. 486–490 (2012).

20. Du, Z., Wen, X., Zhao, D., et al. "Numerical analysis of partial abrasion of the straddle-type monorail vehicle running tyre", *Transactions of Famena*, **41**(1), pp. 99–112 (2017).

21. Xu, Z., Du, Z., Yang, Z., et al. "Research on vehicle-bridge vertical coupling dynamics of monorail based on multiple road excitations", *Mechanika*, **26**(4), pp. 301–310 (2020).

22. Du, Z.X., Yang, Z., Xu, Z.Z., et al. "The study on nonlinear model of pantograph-catenary coupling system for straddle-type monorail", *Mechanika*, **26**(3), pp. 212–220 (2020).

23. Lee, C.H., Kawatani, M., Kim, C.W., et al. "Dynamic response of a monorail steel bridge under a moving

train", *Journal of Sound and Vibration*, **294**(3), pp. 562–579 (2006).

24. Bao, Y.L., Li, Y.L., and Jiajie, D. "A case study of dynamic response analysis and safety assessment for a suspended monorail system", *International Journal of Environmental Research and Public Health*, **13**(11), p. 1121 (2016).

25. Bao, Y.L., Zhai, W.M., Cai, C.B., et al. "Impact coefficient analysis of track beams due to moving suspended monorail vehicles", *Vehicle System Dynamics*, **60**(2), pp. 653–669 (2020).

26. Cai, C.B., He, Q.L., Zhu, S.Y., et al. "Dynamic interaction of suspension-type monorail vehicle and bridge: Numerical simulation and experiment", *Mechanical Systems & Signal Processing*, **118**, pp. 388–407 (2019).

27. Xu, Z., Du, Z., Yang, Z., et al. "Research on vertical coupling dynamics of monorail vehicle at finger-band", *Urban Rail Transit*, **3**(3), pp. 142–148 (2017).

Biographies

Zhouzhou Xu obtained MSc and PhD degrees from Chongqing Jiaotong University in 2011 and 2022, respectively. Currently, he is a Lecturer at the School of Mechanotronics and Vehicle Engineering of Chongqing Jiaotong University, Chongqing, China. His research interests include straddle monorail, intelligent control, and signal analysis.

Zixue Du received the BSc and MSc degrees in Vehicle Engineering from Jilin University, Changchun, China in 1982 and 1995, respectively, and PhD degree in Mechanical Engineering from Southwest Jiao Tong University, Chengdu, China in 2001. He is currently a Professor and PhD supervisor at Chongqing Jiaotong University. From 2005 to 2006, he was a Research visitor at the University of Sheffield, Sheffield, United Kingdom. His research interests include vehicle dynamics and control and straddle type monorail vehicle design and optimization.

Zhen Yang received the BSc degree in Mechanical Engineering from Xinxiang University, Xinxiang, China in 2013, MSc degree in Mechanical Engineering from Chongqing Jiaotong University, Chongqing, China in 2016, and PhD degree in Transport Engineering at Chongqing Jiaotong University, Chongqing, China in 2020. His research interests include vehicle dynamics and control.

Liang Xin received the BE and ME degrees in Aircraft Design and Engineering from Northwestern Polytechnical University, Xi'an, China in 2012 and 2015, respectively, and PhD degree in Transport Engineering at Chongqing Jiaotong University, Chongqing, China in 2021. His research interests include vehicle dynamics and active suspension.